## Title

A Boosted Ensemble Algorithm for Determination of Plaque Stability in High-Risk Patients on Coronary CTA.



## Journal

JACC. Cardiovascular imaging, 13(10)

## ISSN

1936-878X

## Authors

Al'Aref, Subhi J
Singh, Gurpreet
Choi, Jeong W
et al.

## Publication Date

2020-10-01

## DOI

10.1016/j.jcmg.2020.03.025

Peer reviewed

JACC: CARDIOVASCULAR IMAGING VOL. ■, NO. ■, 2020

PUBLISHED BY ELSEVIER

CLINICAL RESEARCH

# A Boosted Ensemble Algorithm for Determination of Plaque Stability in High-Risk Patients on Coronary CTA

Subhi J. Al'Aref, MD,[a] Gurpreet Singh, PhD,[b] Jeong W. Choi, MD,[c] Zhuoran Xu, MD,[c] Gabriel Maliakal, MSc,[d] Alexander R. van Rosendael, MD,[c] Benjamin C. Lee, PhD,[c] Zahra Fatima, BS,[c] Daniele Andreini, MD, PhD,[e] Jeroen J. Bax, MD, PhD,[f] Filippo Cademartiri, MD, PhD,[g] Kavitha Chinnaiyan, MD,[h] Benjamin J.W. Chow, MD,[i] Edoardo Conte, MD,[e] Ricardo C. Cury, MD,[j] Gudruf Feuchtner, MD,[k] Martin Hadamitzky, MD,[l] Yong-Jin Kim, MD,[m] Sang-Eun Lee, MD,[n,o] Jonathon A. Leipsic, MD,[p] Erica Maffei, MD,[q] Hugo Marques, MD,[r] Fabian Plank, MD,[s] Gianluca Pontone, MD, PhD,[e] Gilbert L. Raff, MD,[h] Todd C. Villines, MD,[t] Harald G. Weirich, MD,[s] Iksung Cho, MD,[n,u] Ibrahim Danad, MD,[v] Donghee Han, MD,[w] Ran Heo, MD,[x] Ji Hyun Lee, MD,[w,y] Asim Rizvi, MD,[z] Wijnand J. Stuijfzand, MD,[c] Heidi Gransar, MSc,[aa] Yao Lu, MSc,[c] Ji Min Sung, PhD,[w] Hyung-Bok Park, MD,[w] Daniel S. Berman, MD,[bb] Matthew J. Budoff, MD,[cc] Habib Samady, MD,[dd] Peter H. Stone, MD,[ee] Renu Virmani, MD,[ff] Jagat Narula, MD, PhD,[gg] Hyuk-Jae Chang, MD, PhD,[n] Fay Y. Lin, MD,[c] Lohendran Baskaran, MD,[c,hh] Leslee J. Shaw, PhD,[c] James K. Min, MD[d]

## ABSTRACT

**OBJECTIVES** This study sought to identify culprit lesion (CL) precursors among acute coronary syndrome (ACS) patients based on qualitative and quantitative computed tomography–based plaque characteristics.

**BACKGROUND** Coronary computed tomography angiography (CTA) has been validated for patient-level prediction of ACS. However, the applicability of coronary CTA to CL assessment is not known.

**METHODS** Utilizing the ICONIC (Incident COroNary Syndromes Identified by Computed Tomography) study, a nested case-control study of 468 patients with baseline coronary CTA, the study included ACS patients with invasive coronary angiography–adjudicated CLs that could be aligned to CL precursors on baseline coronary CTA. Separate blinded core laboratories adjudicated CLs and performed atherosclerotic plaque evaluation. Thereafter, the study used a boosted ensemble algorithm (XGBoost) to develop a predictive model of CLs. Data were randomly split into a training set (80%) and a test set (20%). The area under the receiver-operating characteristic curve of this model was compared with that of diameter stenosis (model 1), high-risk plaque features (model 2), and lesion-level features of CL precursors from the ICONIC study (model 3). Thereafter, the machine learning (ML) model was applied to 234 non-ACS patients with 864 lesions to determine model performance for CL exclusion.

**RESULTS** CL precursors were identified by both coronary angiography and baseline coronary CTA in 124 of 234 (53.0%) patients, with a total of 582 lesions (containing 124 CLs) included in the analysis. The ML model demonstrated significantly higher area under the receiver-operating characteristic curve for discriminating CL precursors (0.774; 95% confidence interval [CI]: 0.758 to 0.790) compared with model 1 (0.599; 95% CI: 0.599 to 0.599; $p < 0.01$), model 2 (0.532; 95% CI: 0.501 to 0.563; $p < 0.01$), and model 3 (0.672; 95% CI: 0.662 to 0.682; $p < 0.01$). When applied to the non-ACS cohort, the ML model had a specificity of 89.3% for excluding CLs.

**CONCLUSIONS** In a high-risk cohort, a boosted ensemble algorithm can be used to predict CL from non-CL precursors on coronary CTA. (J Am Coll Cardiol Img 2020;■:■–■) © 2020 by the American College of Cardiology Foundation.

From the [a]Division of Cardiology, Department of Medicine, University of Arkansas for Medical Sciences, Little Rock, Arkansas; [b]GlaxoSmithKline, Brentford, United Kingdom; [c]Department of Radiology, New York-Presbyterian Hospital and Weill Cornell Medicine, New York, New York; [d]Cleerly Health, New York, New York; [e]Centro Cardiologico Monzino, Institute for Research Hospitalization, and Health Care, Milan, Italy; [f]Department of Cardiology, Leiden University Medical Center, Leiden, the Netherlands; [g]Cardiovascular Imaging Center, Institute of Diagnostic and Nuclear Development, Institute for Research Hospitalization, and Health Care, Naples, Italy; [h]Department of Cardiology, William Beaumont Hospital, Royal Oak, Michigan;

ISSN 1936-878X/$36.00 https://doi.org/10.1016/j.jcmg.2020.03.025

**ABBREVIATIONS AND ACRONYMS**

**ACS** = acute coronary syndrome

**APCs** = atherosclerotic plaque characteristics

**AUC** = area under the receiver-operating characteristic curve

**CAD** = coronary artery disease

**CI** = confidence interval

**CL** = culprit lesion

**CTA** = computed tomography angiography

**HU** = Hounsfield unit

**ICA** = invasive coronary angiography

**LAP** = low-attenuation plaque

**MI** = myocardial infarction

**ML** = machine learning

Acute coronary syndrome (ACS) occurs as a result of the predisposition of atherosclerotic plaque to progression and subsequent transformation into high-risk unstable lesions (1,2). Prospective natural history studies of coronary atherosclerosis have sought to elucidate patient-specific and lesion-specific characteristics of vulnerable plaques (3,4). The existent paradigm is based on the fact that ACS arises from plaque with certain histopathologic and hemodynamic characteristics, and that such characteristics can be independent of the traditional measure of diameter stenosis (5,6). Furthermore, recent advances in imaging techniques have permitted the cross-sectional imaging of the coronary vasculature, which has been shown to correlate with histopathologic findings (7). For instance, invasive intravascular ultrasound imaging has been used to define coronary vessel wall anatomy as well as to provide an accurate assessment of atherosclerotic plaque (8). The PROSPECT (Providing Regional Observations to Study Predictors of Events in the Coronary Tree) study used intravascular ultrasound imaging after percutaneous coronary intervention and found that the presence of plaque burden ≥70% and minimal lumen area ≤4.0 $mm^2$ and the occurrence of intravascular ultrasound-determined thin-cap fibroatheroma were independently associated with the incidence of future events within an ACS cohort (3). Yet, despite the improved understanding of coronary artery disease (CAD) pathophysiology coupled with increasingly accurate population-based risk stratification tools, coronary heart disease and the occurrence of unheralded ACS remains a major public health concern (9,10).

Recently, coronary computed tomography angiography (CTA) has been established as an accurate method for the noninvasive evaluation of CAD (11). Coronary CTA has evolved into a comprehensive noninvasive method for the whole-heart assessment of qualitative and quantitative atherosclerotic plaque features, with spatial resolution mirroring that of the invasive reference standard (12). Additionally, coronary CTA-based atherosclerotic plaque characteristics (APCs) and quantitative computed tomography measurements demonstrate incremental prognostic value for patient-level prediction of ACS events (13). However, the applicability of coronary CTA risk prediction to culprit lesion (CL) precursors is not known. We

[i]Department of Medicine and Radiology, University of Ottawa, Ottawa, Canada; [j]Department of Radiology, Miami Cardiac and Vascular Institute, Miami, Florida; [k]Department of Radiology, Medical University of Innsbruck, Innsbruck, Austria; [l]Department of Radiology and Nuclear Medicine, German Heart Center Munich, Munich, Germany; [m]Department of Internal Medicine, Seoul National University Hospital, Seoul, South Korea; [n]Division of Cardiology, Severance Cardiovascular Hospital and Severance Biomedical Science Institute, Yonsei University Health System, Yonsei University College of Medicine, Seoul, South Korea; [o]Yonsei-Cedars-Sinai Integrative Cardiovascular Imaging Research Center, Yonsei University Health System, Yonsei University College of Medicine, South Korea; [p]Department of Medicine and Radiology, University of British Columbia, Vancouver, Canada; [q]Department of Radiology, ASUR Marche Area Vasta 1, Urbino, Italy; [r]Cardiovascular Imaging Unit, Unit of Cardiovascular Imaging, Hospital da Luz, Lisbon, Portugal; [s]Department of Radiology, Innsbruck Medical University, Innsbruck, Austria; [t]Division of Cardiovascular Medicine, Department of Medicine, University of Virginia Health System, Charlottesville, Virginia; [u]Department of Cardiology, Chung-Ang University Hospital, Seoul, South Korea; [v]Department of Cardiology, VU University Medical Center, Amsterdam, the Netherlands; [w]Integrative Cardiovascular Imaging Research Center, Division of Cardiology, Severance Cardiovascular Hospital, Yonsei University College of Medicine, Seoul, South Korea; [x]Division of Cardiology, Department of Internal Medicine, Hanyang University Medical Center, Seoul, Korea; [y]Department of Cardiology, Myongji Hospital, Goyang, South Korea; [z]Department of Radiology, Mayo Clinic, Rochester, Minnesota; [aa]Department of Imaging, Cedars Sinai Medical Center, Los Angeles, California; [bb]Department of Imaging and Medicine, Cedars Sinai Medical Center, Los Angeles, California; [cc]Department of Medicine, Los Angeles Biomedical Research Institute, Torrance, California; [dd]Division of Cardiology, Emory University School of Medicine, Atlanta, Georgia; [ee]Division of Cardiovascular Medicine, Brigham and Women's Hospital, Boston, Massachusetts; [ff]CVPath Institute, Gaithersburg, Maryland; [gg]Marie-Josée and Henry R. Kravis Center for Cardiovascular Health, Zena and Michael A. Wiener Cardiovascular Institute, Mount Sinai Heart, Icahn School of Medicine at Mount Sinai, New York, New York; and the [hh]Department of Cardiovascular Medicine, National Heart Centre, Singapore. This trial was supported by National Institutes of Health Grant No. HL115150 (to Dr. Min) and the Leading Foreign Research Institute Recruitment Program of the National Research Foundation of Korea, Ministry of Science, ICT and Future Planning (Seoul, Korea). The research reported in this manuscript was also supported, in part by, the Dalio Institute of Cardiovascular Imaging (New York, New York). Dr. Signh is an employee of GlaxoSmithKline. Dr. Bax has received speaker fees from Abbott Vascular; and received institutional research grant support from Abbott Vascular, Edwards Lifesciences, Biotronik, Bioventrix, Boston Scientific, Medtronic, and GE Healthcare. Dr. Chinnaiyan has received institutional research grant support and served as a consultant for HeartFlow. Dr. Chow is the Saul and Edna Goldfarb Chair in Cardiac Imaging Research; and has received research grant support from TD Bank, CV Diagnostics and AusculSciences, Siemens Healthineers, and TeraRecon; and owns equity in GE Healthcare. Dr. Cury has served as a consultant for GE Healthcare, Cleerly Health, and Spreemo Health. Dr. Leipsic has served as a consultant for and owns stock options in HeartFlow and Circle CVI; and received research grant support from and served on the Speakers Bureau for GE Healthcare. Dr. Pontone has a

sought to develop a machine learning (ML) prediction model to identify CL precursors based on quantitative computed tomography and APCs among patients with incident ACS using the ICONIC (Incident COroNary Syndromes Identified by Computed Tomography) nested case-control study.

## METHODS

**STUDY POPULATION.** The ICONIC study is a nested case-control study within the international, multi-institutional CONFIRM (COronary CT Angiography EvaluatioN For Clinical Outcomes: An InteRnational Multicenter) registry. Patients from the CONFIRM registry were included in the ICONIC study if they underwent coronary CTA prior to an ACS event and had no prior history of CAD, including a history of prior percutaneous or surgical revascularization. Patients were also excluded from the study if they died without a preceding ACS event. A total of 234 such individuals with ACS were propensity matched 1:1 to same-site control subjects without ACS, for a total of 468 individuals. ACS events were adjudicated by the Clinical and Data Coordinating Center at the Dalio Institute of Cardiovascular Imaging, blinded to coronary CTA findings. Cardiac enzyme measurements, as well as electrocardiograms, were used to adjudicate ACS events according to the World Health Organization definition of myocardial infarction (MI) (14). Coronary CTA-based quantitative and qualitative evaluations were performed by the coronary CTA Core Laboratory at Severance Hospital of Yonsei University, blinded to case status. Both the ICONIC and CONFIRM studies have been described in more detail in previous publications (13,15). Every institution received local review board (Institutional Review Board) or ethics board approval.

Of the 234 patients with ACS, 124 patients were included, for whom invasive coronary angiography (ICA)-adjudicated CLs could be aligned to CL precursors on baseline coronary CTA (**Figure 1**). Patient data including clinical history, laboratory testing, electrocardiograms, and diagnostic coronary angiography films were reviewed by the Clinical and Data Coordinating Center at the Dalio Institute of Cardiovascular Imaging. Among patients with ACS (including non–ST-segment elevation MI or unstable angina) a single lesion was considered culprit if significant stenosis was present. In ACS with multiple lesions of 50% diameter lumen reduction, the CL was identified on the basis of association of angiographic lesion appearance with electrocardiography changes or myocardial ischemia as detected during stress testing. Usually the lesion with the most significant luminal narrowing was identified as the CL. The criteria for MI and unstable angina were the same. Any additional imaging of coronary plaques or follow-on percutaneous coronary intervention was left up to the discretion of the primary operator in accordance to the standard of care. The decision to intervene, if any, was left to the primary operator.

**CORONARY CTA.** Coronary CTAs were performed at multiple participant sites on scanners from various vendors. All scanners had at least 64 detector rows, and imaging protocols followed guidelines set by the Society of Cardiovascular Computed Tomography (16). All images were analyzed by American College of Cardiology level III or equivalent cardiologists or radiologists at the coronary CTA core lab who were blinded to case status. The core lab performed standardized measurements using semiautomated plaque analysis software utilizing the model-guided minimum cost approach (QAngioCT Research Edition version 2.1.9.1, Medis Medical Imaging Systems, Leiden, the Netherlands), with manual correction applied as deemed appropriate by the interpreting physician. For each lesion, quantitative measures were performed of length, volume, plaque burden, and plaque composition (categorized as noncalcified, fibrous, or fibrofatty, and calcified using predetermined Hounsfield unit [HU] thresholds). In addition to the aforementioned volumetric measures,

research grant and/or honorarium as a speaker from GE Healthcare, Bracco, Bayer, Medtronic, and HeartFlow. Dr. Berman has received research grant support from HeartFlow and software royalties from Cedars-Sinai Medical Center. Dr. Budoff received research grant support from the National Institutes of Health and GE Healthcare. Dr. Samady has served as a consultant and received research grant support from Philips; has received institutional research grant support from Abbott Vascular, Medtronic, and Philips; is co-founder of Covanos; and owns equity in Covanos and SIG. Dr. Shaw owns equity in Cleerly Health. Dr. Min has received funding from the Dalio Foundation, the National Institutes of Health, and GE Healthcare; has served on the scientific advisory board of Arineta and GE Healthcare; and previously worked at Weill Cornell Medicine but is now an employee of and owns equity in Cleerly Health. All other authors have reported that they have no relationships relevant to the contents of this paper to disclose.

The authors attest they are in compliance with human studies committees and animal welfare regulations of the authors' institutions and Food and Drug Administration guidelines, including patient consent where appropriate. For more information, visit the *JACC: Cardiovascular Imaging* author instructions page.

Manuscript received February 14, 2020; revised manuscript received March 24, 2020, accepted March 31, 2020.

**FIGURE 1 Flow Chart of the Machine Learning Methodology**

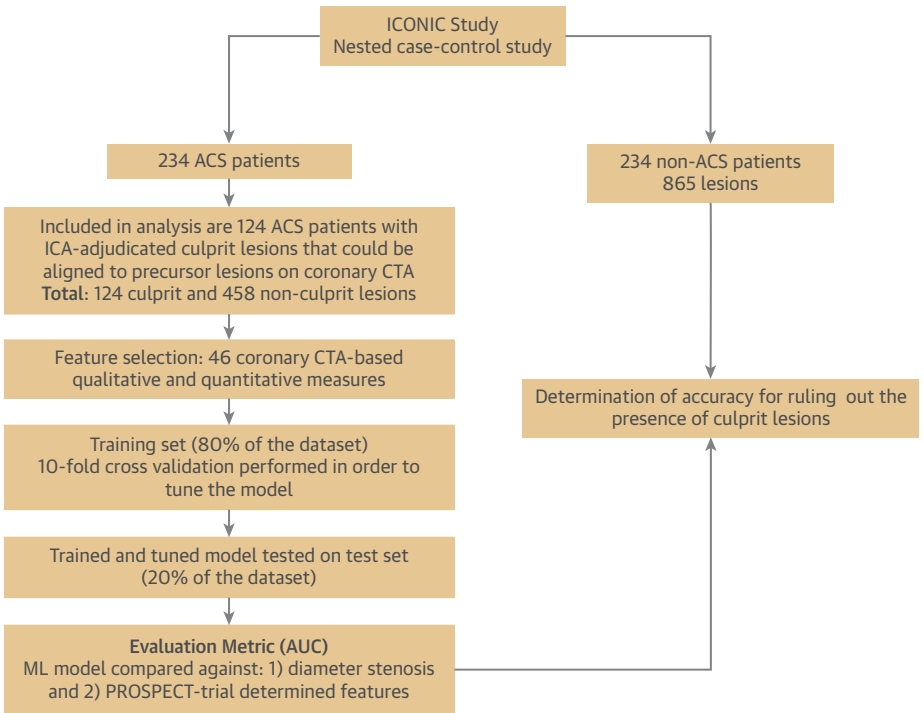


Machine learning model built using a boosted ensemble algorithm (XGBoost), trained and tuned using 10-fold stratified cross-validation. ACS = acute coronary syndrome; AUC = area under the receiver-operating characteristic curve; CTA = computed tomography angiography; ICA = invasive coronary angiography; ML = machine learning; PROSPECT = Providing Regional Observations to Study Predictors of Events in the Coronary Tree.

cross-sectional measures were performed including percent diameter stenosis, area stenosis, minimum luminal diameter, minimal lumen area, cross-sectional plaque burden, and remodeling index. Finally, APCs were categorized as present or absent and included positive remodeling (defined as index ≥1.1), low-attenuation plaque (LAP) (defined as plaque containing any voxel ≤30 HU), spotty calcification (any lesion ≤3 mm) (13), and the napkin-ring sign. ICA-determined CLs were co-registered to the coronary CTA precursor lesions using the distance from coronary ostia as well as bifurcations as fiduciary landmarks.

**MACHINE LEARNING. Model creation and feature selection.** A total of 46 coronary CTA-based qualitative and quantitative plaque features were used in the ML model in order to create a predictive model of CLs (Supplemental Table 1). Models were then built using a boosted ensemble algorithm (XGBoost), using an open-source XGBoost library. XGBoost uses an ensemble of gradient-boosted decision trees, and has been widely applied within the domains of computer science and medicine. The advantage of using a boosted ensemble algorithm is the fact that it can combine multiple weak classifiers to produce a single strong classifier, which can improve prediction modeling. The SHAP (SHapley Additive exPlanations) method was used to explain the output of the ML model. The SHAP method assigns each variable an importance value for a particular prediction, and in this instance was used to order to determine the influence of a particular variable on CL prediction, as well as the direction of that association (17). Such a step provides insight into the inner workings of complex models, such as those created using ensemble methodologies, and strikes a balance between accuracy and interpretability.

**Model training.** The total dataset was split into training (80%) and testing (20%) sets in such a way that the ratio of CLs to non-CLs was maintained. This training set was further split into 10 folds while maintaining the ratio of CLs to non-CLs for grid search of model hyperparameters using 10-fold cross-validation. In this step, the model with a given selection of

**TABLE 1** Baseline Computed Tomography-Based Quantitative and Qualitative Plaque Measures, Stratified by Lesion Status

| | Culprit Lesions (n = 124) | Nonculprit Lesions (n = 458) | p Value |
|---|---|---|---|
| Reference vessel area, $mm^2$ | 8.93 (6.71-14.3) | 6.77 (4.61-10.74) | <0.001 |
| Ostium to MLD lesion distance, mm | 35.300 (21.380-46.510) | 40.860 (26.300-71.760) | 0.0016 |
| Atherosclerotic plaque characteristics, % | | | |
| Positive remodeling | 79.84 | 80.79 | 0.813 |
| Spotty calcification | 18.54 | 13.10 | 0.124 |
| Low-attenuation plaque | 25.00 | 14.63 | 0.006 |
| Napkin-ring sign | 3.23 | 0.66 | 0.040 |
| Lesion length, $mm^2$ | 28.76 (19.64-47.81) | 18.3 (13.35-28.2) | <0.001 |
| Vessel volume (of the lesion), $mm^3$ | 253.24 (136.80-546.17) | 135.36 (70.38-255.65) | <0.001 |
| Lumen volume (of the lesion), $mm^3$ | 173.72 (96.49-318.35) | 98.04 (57.86-181.87) | <0.001 |
| Plaque volume (of the lesion), $mm^3$ | 90.75 (26.51-193.66) | 24.71 (9.64-67.2) | <0.001 |
| Plaque burden, % | 63.25 (43.38-79.34) | 50.14 (35.79-64.78) | <0.001 |
| Fibrous volume (of the lesion), $mm^3$ | 34.30 (12.190-91.70) | 11.27 (4.59-30.69) | <0.001 |
| Fibrofatty volume (of the lesion), $mm^3$ | 8.36 (1.08-30.05) | 1.75 (0.13-9.16) | <0.001 |
| Necrotic core volume (of the lesion), $mm^3$ | 0.15 (0.00-2.36) | 0.00 (0.00-0.34) | <0.001 |
| Dense calcium volume (of the lesion), $mm^3$ | 17.89 (2.25-73.52) | 5.73 (1.38-20.03) | 0.001 |

Values are median (interquartile range) or %, unless otherwise indicated.
MLD = minimal lumen diameter.

hyperparameters was trained on 9 folds and tested on the remaining fold 10 different times so that each fold was used as the test set exactly once. The average of the area under the receiver-operating characteristic curve (AUC) on each test fold was calculated and the set of hyperparameters that led to the highest average AUC was chosen. Using this set of hyperparameters, the model was then trained on the entire training set and evaluated on the test set. We report the AUCs from the test set.

**MODEL PERFORMANCE: RULING IN AND RULING OUT CLs.** The performance of the ML model in predicting CLs was compared with that of diameter stenosis (model 1), high-risk plaque features (model 2), and lesion-level features of CL precursors from the ICONIC study (model 3). Diameter stenosis was categorized according to the recommendations of the Coronary Artery Disease Reporting and Data System consensus document as follows: 0%, 1% to 24%, 25% to 49%, 50% to 69%, 70% to 99%, and 100% occluded (model 1) (18). On coronary CTA, high-risk plaque features included the presence of positive remodeling, LAP, spotty calcification, and the napkin-ring sign (model 2). The ICONIC study had shown that CL precursors, compared with within-subject non-CLs, exhibited higher hazard for diameter stenosis, lesion length, plaque volume, all plaque constituents (calcified, noncalcified, fibrous, fibrofatty, and necrotic core), mean and max plaque burden, high-risk plaque, and LAP (13). Thereafter, these features were used in an XGBoost model to predict CL precursors within the ICONIC study ACS cohort (model 3). Finally, the ML model was applied to the ICONIC non-ACS cohort in order to determine model specificity in ruling out the presence of CLs.

**STATISTICAL ANALYSIS.** Data were analyzed with the use of R version 3.5.0 (RStudio, Boston, Massachusetts) and Python (Python Software Foundation, Beaverton, Oregon). Continuous variables were expressed as median (interquartile range), whereas categorical variables were expressed as count and percentage. Differences between continuous and categorical variables were analyzed by the Wilcoxon rank sum test, chi-square test, and Fisher exact test as appropriate. Subsequent computed tomography-based comparison models were created to include diameter stenosis (model 1), high-risk plaque features (model 2), and lesion-level features of CL precursors from the ICONIC study (model 3) for the prediction of CLs, with the AUC and the associated 95% confidence interval (CI) used for comparison of the different models. All tests were 2-sided and conducted at the 0.05 significance threshold, while the different models were compared using the corrected p value threshold for multiple comparisons (p per number of comparisons) (3).

## RESULTS

The study cohort comprised of 124 individuals with ACS, with a total of 582 coronary plaques, of which 124 were ICA-determined CLs that were co-registered to precursor lesions on coronary CTA (median time between coronary CTA and first ACS event was 34.50

**FIGURE 2 Prediction of Culprit Lesion Precursors Across Four Different Models**

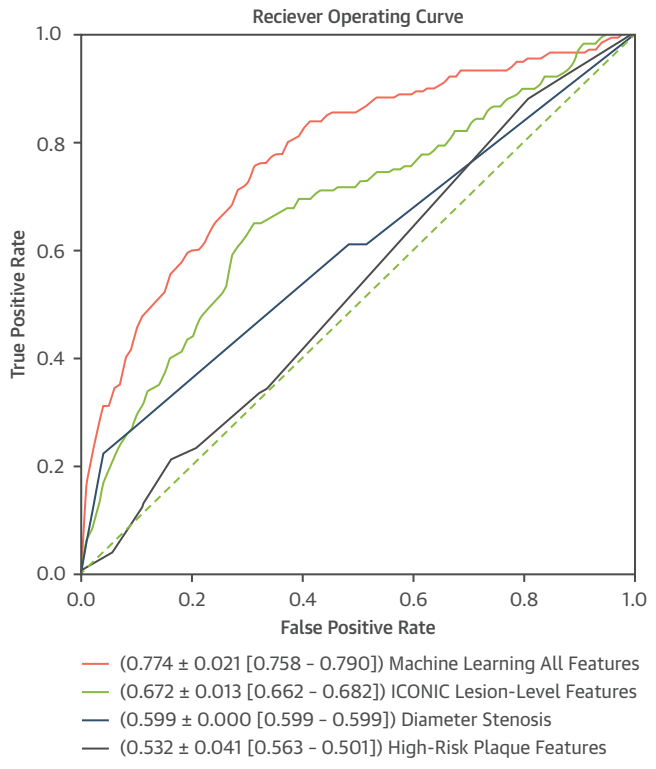


Performance of the ML model in terms of culprit lesion prediction, using AUC, compared with diameter stenosis, high-risk plaque features, and lesion-level features of culprit lesion precursors from the ICONIC (Incident COroNary Syndromes Identified by Computed Tomography) study. The ML model shows better performance for discrimination of culprit lesion precursors compared with the other models. MLD = minimal lumen diameter; other abbreviations as in Figure 1.

[interquartile range: 3.25 to 430.00] days). Of the 124 patients, 38 (30.6%) fulfilled the World Health Organization criteria for MI (ST-segment elevation MI and non-ST-segment elevation MI), and 86 (69.4%) were classified as unstable angina. The mean age was 62.6 ± 11.3 years, and 82 (66.1%) were men. In terms of prevalent cardiovascular conditions, 78 (62.9%) individuals had hypertension, 73 (58.9%) had hyperlipidemia, 31 (25.0%) had diabetes mellitus, and 34 (27.4%) were active smokers. With respect to clinical presentation, 95 (76.6%) presented with chest pain, of which 34 (35.8%) had typical anginal chest pain. There were significant baseline differences in quantitative and qualitative plaque measures between CLs and non-CLs (Table 1). Characteristics of patients with ACS excluded from the analysis have been summarized (Supplemental Table 2).

**PREDICTION OF CLs.** A total of 46 coronary CTA-based qualitative and quantitative plaque features were used in the constructed ML model for CL prediction. The ML model exhibited a significantly higher AUC for discriminating CL precursors (0.774; 95% CI: 0.758 to 0.790) compared with model 1 (0.599; 95% CI: 0.599 to 0.599; $p < 0.01$), model 2 (0.532; 95% CI: 0.501 to 0.563; $p < 0.01$), and model 3 (0.672; 95% CI: 0.662 to 0.682; $p < 0.01$) (Figure 2). Figure 3 shows feature importance ranking for the ML model for prediction of CLs, with quantitative plaque features, as determined on coronary CTA, occupying 19 of the top 20 most significant features. The distance between the start of a lesion and the minimal lumen diameter was the highest-ranked predictor of CLs, followed by plaque volume, luminal area stenosis, plaque burden in maximal stenosis section, and dense calcium volume (>350 HU). The segment where an atherosclerotic lesion starts was the only ordinal variable in the top 20 features, while none of the high-risk plaque features were among the most predictive features.

SHAP assigns each variable an importance value for CL prediction, as well as the direction of that association. SHAP provides information not only about how important a feature is in a particular prediction (vertical position), but also about whether the feature value was high or low for that dataset (color), and also whether the effect of that value resulted in a higher prediction (CL prediction) or lower prediction (non-CL prediction) (horizontal position). For example, higher values for the top feature (start of a lesion to minimal lumen diameter) were predictive of CL precursors, indicating that the length and location of baseline plaque influenced short-term plaque stability. Further, higher plaque burden was predictive of CL precursors, while lower plaque burden was predictive of being a non-CL (Figure 3). According to the feature ranking done by SHAP, baseline plaque location ("Shape of a lesion to minimal lumen diameter") and plaque volume factored higher than baseline luminal area stenosis in the maximal stenosis section. Quantitative descriptors of plaque composition such as dense calcium volume, dense calcium area, fibrous plaque volume, and fibrous fatty plaque area were all in the top 20 important features of CLs.

Subgroups were stratified by age (≥65 or <65 years), sex (male vs. female), and coronary vessel (left anterior descending artery vs. left circumflex artery vs. right coronary artery) (Table 2). The ML model was statistically superior to all computed tomography-based models in CL determination across most subgroups, with the exception of female patients, in which diameter stenosis (model 1) was superior to the

**FIGURE 3** **Feature Importance Ranking of the Machine Learning Model for Culprit Lesion Prediction**

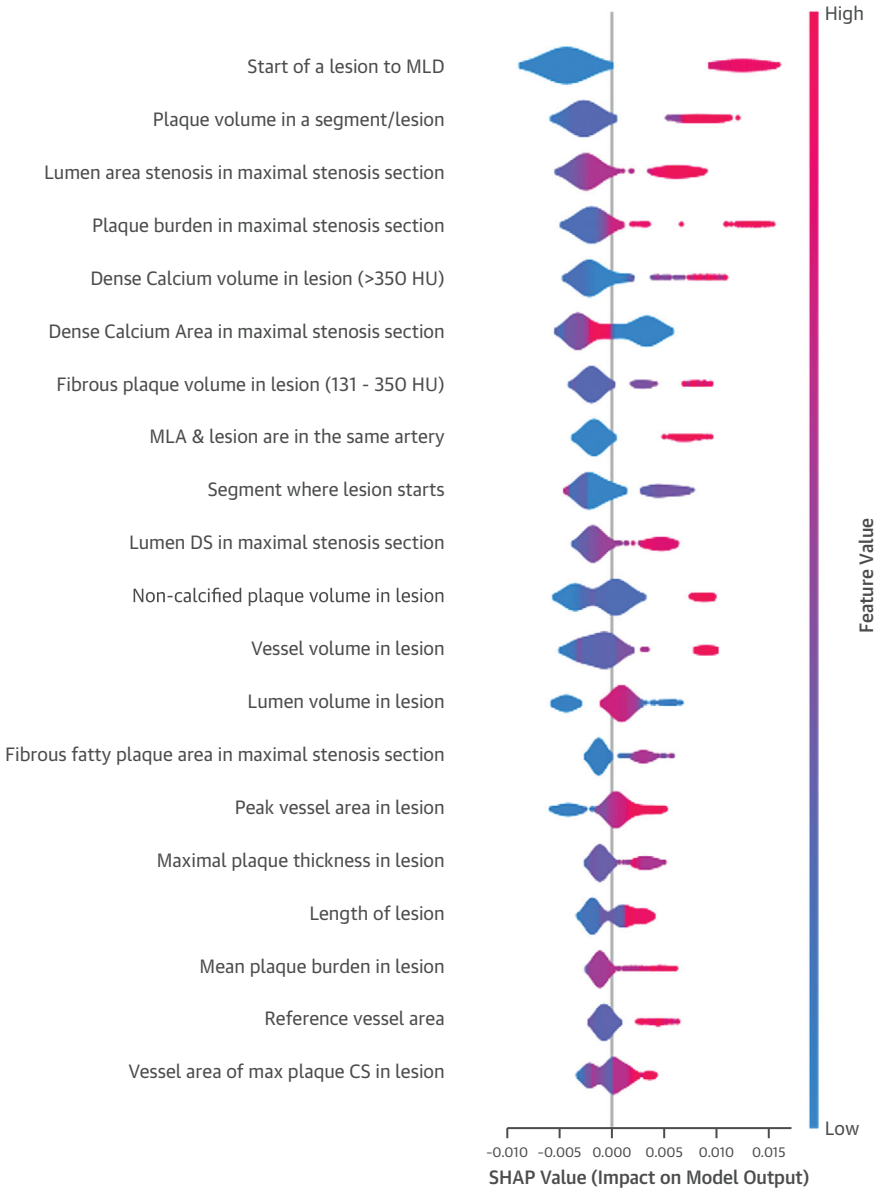


Quantitative and qualitative plaque features are arranged in descending order of importance for culprit lesion prediction. The x-axis provides the SHAP (SHapley Additive exPlanations) method value, which is a measure of the impact of the variable value on the specified prediction (in this case, culprit lesion prediction). **Blue and red points in each row** represent low to high values of the specific variable. CS = cross-section; DS = diameter stenosis; HU = Hounsfield unit; MLA = minimal lumen area; MLD = minimal lumen diameter.

ML model for prediction of CL precursors (AUC: 0.748 vs. 0.835; $p < 0.01$). In addition, lesion-level features of CL precursors from the ICONIC study (model 3) were superior to the ML model in predicting CLs in the right coronary artery (AUC: 0.858 vs. 0.714; $p < 0.01$). Model 2 incorporating high-risk plaque features performed poorly across all subgroups.

**RULING OUT NON-CLs.** The non-ACS ICONIC study cohort, comprising 234 individuals with 864 lesions, was used in order to evaluate the performance of the ML model in ruling out the presence of CLs. The non-ACS cohort had a mean age of 62.4 ± 11.0 years and 146 (62.4%) were men, while 124 (53.0%) had chest pain. A total of 169 (72.2%) individuals had

**TABLE 2 Subgroup Analysis Comparing the Performance of the Machine Learning Model With Diameter Stenosis, High-Risk Plaque, and ICONIC Study Lesion-Level Model**

| Subgroup (Number of Lesions) | Machine Learning AUC | ICONIC Lesion-Level AUC | p Value | Diameter Stenosis AUC | p Value | High-Risk Plaque AUC | p Value |
|---|---|---|---|---|---|---|---|
| Overall | 0.774 ± 0.021 (0.758-0.789) | 0.672 ± 0.013 (0.662-0.682) | <0.01 | 0.599 ± 0.000 (0.599-0.599) | <0.01 | 0.531 ± 0.040 (0.500-0.563) | <0.01 |
| Age ≥65 yrs (n = 62) | 0.796 ± 0.026 (0.776-0.816) | 0.721 ± 0.016 (0.708-0.733) | <0.01 | 0.720 ± 0.000 (0.720-0.720) | <0.01 | 0.506 ± 0.030 (0.483-0.530) | <0.01 |
| Age <65 yrs (n = 55) | 0.739 ± 0.027 (0.718-0.760) | 0.594 ± 0.024 (0.576-0.613) | <0.01 | 0.545 ± 0.001 (0.544-0.545) | <0.01 | 0.552 ± 0.079 (0.492-0.611) | <0.01 |
| Male (n = 88) | 0.780 ± 0.023 (0.763-0.798) | 0.661 ± 0.015 (0.650-0.673) | <0.01 | 0.533 ± 0.000 (0.533-0.533) | <0.01 | 0.542 ± 0.032 (0.518-0.567) | <0.01 |
| Female (n = 29) | 0.748 ± 0.044 (0.715-0.781) | 0.701 ± 0.035 (0.674-0.728) | <0.01 | 0.835 ± 0.000 (0.835-0.835) | <0.01 | 0.502 ± 0.071 (0.449-0.552) | <0.01 |
| Left anterior descending artery (n = 58) | 0.795 ± 0.015 (0.783-0.807) | 0.712 ± 0.018 (0.698-0.726) | <0.01 | 0.564 ± 0.000 (0.564-0.564) | <0.01 | 0.556 ± 0.032 (0.531-0.580) | <0.01 |
| Left circumflex artery (n = 27) | 0.751 ± 0.061 (0.705-0.797) | 0.350 ± 0.051 (0.311-0.388) | <0.01 | 0.660 ± 0.000 (0.660-0.660) | <0.01 | 0.226 ± 0.138 (0.120-0.328) | <0.01 |
| Right coronary artery (n = 32) | 0.714 ± 0.039 (0.684-0.743) | 0.858 ± 0.040 (0.828-0.888) | <0.01 | 0.644 ± 0.000 (0.644-0.644) | <0.01 | 0.437 ± 0.043 (0.404-0.469) | <0.01 |

Values are mean ± SD (range). Numbers are reported on the validation set. The p values are for comparison between the specific model and the machine learning model.
AUC = area under the receiver-operating characteristic curve; ICONIC = Incident COroNary Syndromes Identified by Computed Tomography.

obstructive CAD on coronary CTA, defined as any vessel with >50% diameter stenosis, as a result of the propensity matching criteria within the ICONIC study cohort (ACS to non-ACS individuals were matched on clinical risk factors and CAD severity). The median follow-up after coronary CTA performance was 865 (interquartile range: 597 to 1,497) days. The model had a specificity of 89.3% for predicting non-CLs (the model predicted 93 of 864 lesions as being CLs although, in fact, they were non-CLs). In terms of misclassified lesions (i.e., lesions that were incorrectly predicted as CLs by the ML model), the ML model tended to misclassify longer lesions, with heavier plaque burden (including both calcified and noncalcified components) and lesions in larger vessels. Table 3 lists differences in computed tomography-based quantitative plaque characteristics between correctly predicted non-CLs and lesions incorrectly predicted as CLs by the ML model.

## DISCUSSION

The current study utilized coronary CTA-determined quantitative and qualitative atherosclerotic plaque features within a cohort of individuals with subsequent incident ACS, and developed a model for the prediction of CLs with better accuracy than a model that featured diameter stenosis, computed tomography-determined high-risk plaque features, as well as lesion-level characteristics of CL precursors. These results were consistent across certain subgroups while the most predictive features were quantitative features. The unexpected finding regarding the poor performance of high-risk plaque for CL discrimination could be secondary to the fact that the derivation cohort included ACS patients, with previous investigations showing that even though high-risk plaque was an independent predictor of ACS, the cumulative number of lesions with and without high-risk plaque was similar in ACS cohorts, as compared with the low incidence of high-risk plaque in a non-ACS cohort (in our cohort, 40 of 126 [32.0%] of CLs had high-risk plaque, whereas 93 of 458 [20.3%] of the non-CLs had high-risk plaque) (19). The results of the present analysis are important, as they provide a better understanding of the relationship between computed tomography-determined plaque features (in terms of both qualitative and quantitative measures) and the presence of CL precursors in a high-risk cohort, albeit over a median follow-up interval of 865 days. It also provides a model featuring quantitative and qualitative plaque characteristics that can be used to determine plaque stability in a non-ACS cohort.

Prior to the inception and adoption of invasive and noninvasive coronary imaging, a significant body of knowledge on the natural history of coronary atherosclerosis came from pathology studies demonstrating that an ACS event occurs as a result of atherosclerotic plaque erosion or rupture, which frequently occurs in the setting of thin-cap fibroatheromas that are characterized by the presence of a large necrotic core and covered with a thin fibrous cap (<65 μm) separating it from the coronary lumen (5). The identification of thin-cap fibroatheromas within the context of vulnerable plaque and

**TABLE 3 Differences in Computed Tomography–Based Plaque Characteristics Between Correctly Predicted Non-CLs and Those Incorrectly Predicted as CLs by the Machine Learning Model**

| Plaque Characteristic | Correctly Classified Non-CLs (n = 773) | Incorrectly Classified Non-CLs (n = 93) | p Value |
|---|---|---|---|
| Plaque volume in segment/lesion | 25.3 (9.4–70.1) | 116.2 (46.3–269.4) | <0.05 |
| Plaque burden in maximal stenosis section | 47.1 (33.8–61.5) | 69.6 (52.4–79.5) | <0.05 |
| Dense calcium volume in lesion | 7.0 (1.5–22.7) | 41.2 (9.8–93.2) | <0.05 |
| Dense calcium area in maximal stenosis section | 0.6 (0.0–2.1) | 1.2 (0.0–6.2) | <0.05 |
| Fibrous plaque volume in lesion | 11.8 (4.0–29.7) | 47.7 (20.7–269.4) | <0.05 |
| Lumen diameter stenosis in maximal stenosis section | 20.6 (11.7–32.1) | 36.6 (27.1–46.5) | <0.05 |
| Noncalcified plaque volume in lesion | 15.2 (4.8–39.0) | 61.1 (9.8–93.2) | <0.05 |
| Vessel volume in lesion | 133.3 (70.0–261.8) | 397.3 (162–638.2) | <0.05 |
| Lumen volume in lesion | 102.6 (55.8–191.5) | 239.4 (104.5–371.6) | <0.05 |
| Fibrous fatty plaque area in maximal stenosis section | 0.1 (0.0–1.0) | 0.4 (0.0–2.6) | <0.05 |
| Peak vessel area in lesion | 9.9 (6.7–14.3) | 15.9 (11.5–20.0) | <0.05 |
| Maximal plaque thickness in lesion | 1.6 (1.2–2.0) | 2.2 (1.9–2.7) | <0.05 |
| Length of lesion | 18.41 (13.7–29.5) | 34.6 (20.1–56.9) | <0.05 |
| Mean plaque burden in lesion | 17.8 (10.2–28.3) | 31.1 (20.6–42.1) | <0.05 |
| Reference vessel area | 7.2 (4.9–11.3) | 10.8 (8.2–14.3) | <0.05 |
| Vessel area of maximal plaque cross-section in lesion | 9.2 (6.1–12.9) | 13.9 (10.1–17.4) | <0.05 |

Values are median (interquartile range).
CL = culprit lesion.

unheralded acute MI raised the possibility of improved risk stratification above and beyond population-derived risk scores that are based on classical risk-factor profiles. As such, there has been keen interest in developing catheter-based imaging techniques for the detection of various anatomic components of thin-cap fibroatheromas, as well as metabolic processes of high-risk plaque, culminating in the application of intravascular ultrasound, near-infrared spectroscopy, and optical coherence tomography to visualize and characterize atherosclerotic plaque. For instance, the PROSPECT trial enrolled 697 patients with ACS who underwent 3-vessel coronary angiography as well as imaging after percutaneous coronary intervention (3). The PROSPECT trial showed that lesions at enrollment that were associated with subsequent events, at a median follow-up period of 3.4 years, were characterized by a minimal luminal area of ≤4.0 $mm^2$ and plaque burden of ≥70%, or were identified as thin-cap fibroatheromas. The VIVA (Virtual Histology in Vulnerable Atherosclerosis) study enrolled 170 patients with stable angina or troponin-positive ACS who underwent 3-vessel intravascular ultrasound (a total of 30,372 mm of intravascular ultrasound analyzed) and evaluated the association between intravascular ultrasound-identified thin-cap fibroatheromas and major adverse cardiac events (20). Thin-cap fibroatheromas was associated with major adverse cardiac events on individual plaque analysis, while noncalcified thin-cap fibroatheromas was associated with major adverse cardiac events on a patient-level analysis. Similar to intravascular ultrasound, studies using optical coherence tomography suggest that fibrous cap thickness is an important distinguishing feature between ruptured and nonruptured thin-cap fibroatheromas, while plaque burden and luminal area were features associated with ruptured culprit plaque (21). One major criticism of the aforementioned investigations is that "events" were driven by revascularization, which could explain why features such as plaque burden and minimal lumen area correlated with adverse events. In the present analysis, events were core lab-adjudicated ACS events, especially in patients with unstable angina who were judged based on World Health Organization criteria and not based on revascularization decisions.

Coronary CTA-determined qualitative and quantitative measures have been shown to correlate with the occurrence of ischemia and adverse cardiovascular events. Further, the incremental prognostic value of coronary CTA-determined APCs has been further validated within large multicenter prospective trials (22). In a prespecified analysis of the PROMISE (Prospective Multicenter Imaging Study for Evaluation of Chest Pain) trial, 4,415 symptomatic patients but with stable chest pain underwent baseline coronary CTA and had the presence of high-risk plaque determined by a core lab. The presence of high-risk plaque was associated with a higher rate of major adverse cardiovascular events (6.4% vs. 2.4%; hazard ratio: 2.73; 95% CI: 1.89 to 3.93), even after adjustment for traditional risk scores. Similar analysis with the

**CENTRAL ILLUSTRATION** **Integration of Coronary Computed Tomography Angiography-Determined Atherosclerotic Plaque Features With Machine Learning Algorithms for the Development of a Prediction Model of Culprit Lesion Precursors**

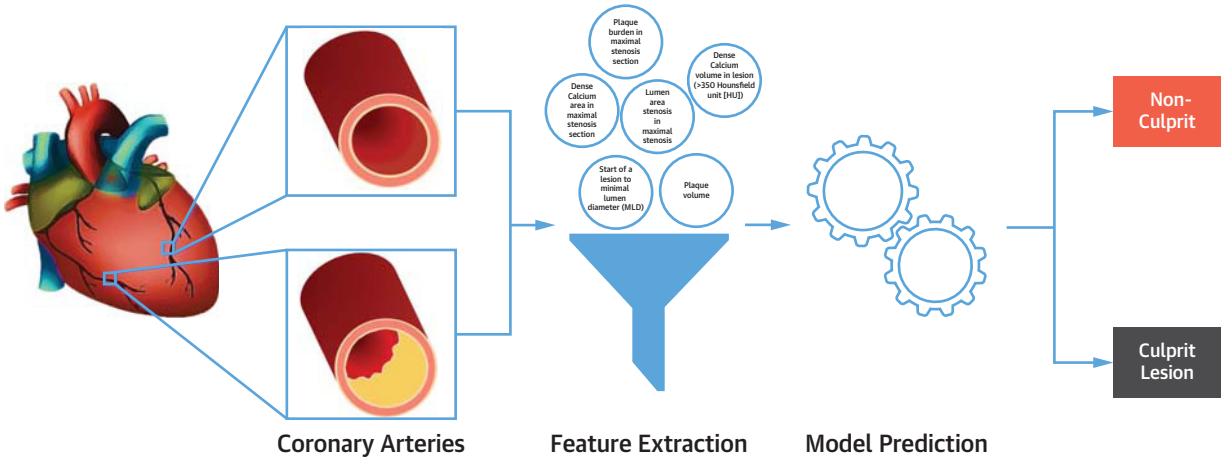


**Al'Aref, S.J. et al. J Am Coll Cardiol Img. 2020;■(■):■–■.**

The aforementioned approach could provide a method for determination of atherosclerotic plaque stability, which could help with therapy selection and downstream testing.

ROMCAT II (Rule Out Myocardial Infarction/Ischemia Using Computer-Assisted Tomography II) trial showed that the presence of high-risk plaque on coronary CTA was associated with adverse events (odds ratio: 8.9; 95% CI: 1.8 to 43.3; $p = 0.006$). Such findings highlight the potential of coronary CTA-based atherosclerotic plaque characterization for risk assessment that encompasses overall measures of atherosclerotic plaque burden, as well as lesion-specific APCs. In the present study, quantitative measures of plaque burden played a larger role in the prediction of CLs when compared with plaque characteristics. This may be due to the proportionally larger number of quantitative variables included in this study, some of which may be co-associated. As the assessment of vulnerable plaque has progressed from identification to volumetric quantification, future studies incorporating volumetric vulnerable plaque assessment may further elucidate and enhance the prediction of CLs. Such extensive plaque characterization could embellish the drive toward precision medicine, wherein cardiovascular care moves from being a global risk-assessment field with population-derived clinical risk profiles into one that incorporates accurate phenotypic plaque characterization that precisely predicts at-risk individuals through the detection of vulnerable plaque (**Central Illustration**).

There is an increasing need for improved detection and discrimination between stable and vulnerable plaque on noninvasive imaging studies. Current European guidelines consider the presence of multivessel CAD with 2 major epicardial vessels having >50% stenosis as very high risk, necessitating the institution of aggressive lipid-lowering therapy (23). Although increasing diameter stenosis portends higher risk, only 24.8% of the culprit precursors in the ICONIC study were obstructive (diameter stenosis ≥50%), thus highlighting the importance of whole plaque evaluation. ML, which employs mathematical modeling to examine for multidimensional associations between certain features, has been increasingly used, on a per-patient level, for the prediction of adverse cardiovascular events using both structured clinical and imaging data (Supplemental Table 3). ML can be particularly useful for identifying imaging markers of plaque vulnerability that significantly outperform conventional quantitative and qualitative computed tomography-based high-risk plaque features (24,25). This is particularly essential because plaque characteristics display complex inter-relationships that may be hard to model with simple regression-based methodologies. Furthermore, deep learning algorithms, which use methods based on learning data representations, are aptly suited for image analysis and can be utilized for

examining plaque characteristics that are impossible to capture in structured reports or even within human vision (e.g., shape, location, and relationship to other structures, in addition an extensive assessment of pixel-by-pixel variations as it relates to a specific plaque phenotype or clinical outcome).

**STUDY LIMITATIONS.** Despite the novelty of the conducted investigation, there are certain limitations that are noteworthy to mention. As previously described, individuals with ACS within the ICONIC study cohort had been selected from the larger observational CONFIRM registry investigation. As such, there could be unmeasured confounders with respect to patient selection as well as potentially other biases regarding the propensity-matching approach employed within the ICONIC study cohort, hence limiting the generalizability of the present findings. For example, the proximity of ACS events after CTA acquisition indicates that this referral population is at higher risk than the general population. Further, the impact of coronary CTA on decision making, including changes in medical therapy, is unclear. Thus, the current findings are mainly limited to a higher-risk patient population and cannot be generalized to stable angina or even asymptomatic patients. Second, quantitative plaque and luminal measures were performed with a semiautomated software (QAngio CT Research Edition version 2.1.9.1), a process that is laborious and not easily reproducible. Third, the median follow-up period after coronary CTA performance was 865 days, which is fairly short, especially when the endpoint is the occurrence of an ACS event on a patient level and the development of unstable plaque on a lesion level. It is possible that non-CLs could become culprits over longer follow-up, and it is uncertain whether the same plaque characteristics influence long-term plaque stability. Fourth, the results of the present study were not externally validated on a separate cohort. However, no cohort exists in which a primary prevention cohort underwent extensive baseline coronary CTA-derived qualitative and quantitative plaque assessment for suspected CAD and subsequently had CL adjudication on ICA as well as co-registration of CLs to the coronary CTA precursor lesions. Last, this study was limited to CLs that could be identified by a clinical committee, with the presence of significant diameter stenosis on ICA being the major driver for determining the presence of a CL. As such, the performance of this model in the setting of CLs that are nonobstructive, or lesions that lead to clinically silent events, is not known.

The results of present analysis have several important clinical implications. First, with the increasing wealth of knowledge regarding the influence of qualitative and quantitative plaque analysis for future cardiovascular event prediction, there is an unmet need for advanced analytic approaches for data processing as well as precise and patient-tailored risk prediction. ML has been applied for assimilation of complex datasets for patient-level risk prediction, and this study shows that it is possible to integrate a multitude of qualitative and quantitative plaque characteristics for prediction of plaque stability. Second, there is inconsistency and significant variability regarding the acceptable definitions for high-risk plaque, with often arbitrary cutoff values used to define the presence or absence of such features. Our approach plots the influence of each value on the prediction of plaque stability, using the SHAP method, which can be used as a platform in future analysis for refined and more precise definition of high-risk features. Third, the ability to predict likely CLs in symptomatic high-risk patients could be useful for therapy selection and downstream testing. For instance, if the ML model predicts that a left main or proximal left anterior descending artery plaque might become a culprit, then a clinician may consider aggressive preventative therapies, regular follow-up, and performance of invasive evaluation in the setting of breakthrough symptoms. However, the utility of such an approach needs to be supported by evidence from clinical trials.

## CONCLUSIONS

In summary, an ML approach incorporating coronary CTA-determined qualitative and quantitative plaque features was better at predicting CL precursors compared with diameter stenosis or computed tomography-determined high-risk plaque features and was robust across several subgroups. Furthermore, it was accurate in ruling out the presence of CL precursors in a non-ACS cohort. This study highlights the utility of ML for predicting culprit from non-CL precursors in a high-risk cohort on coronary CTA.

**ADDRESS FOR CORRESPONDENCE:** Dr. Subhi J. Al'Aref, Division of Cardiology, Department of Medicine, University of Arkansas for Medical Sciences. 4301 West Markham Street, Little Rock, Arkansas 72205. E-mail: SJAlaref@UAMS.edu.

## PERSPECTIVES

**COMPETENCY IN MEDICAL KNOWLEDGE:** An ML model that integrates coronary CTA–determined qualitative and quantitative plaque features showed improved detection of CL precursors in a high-risk cohort compared with contemporary risk assessment methods, and was robust across several subgroups including younger individuals (<65 years of age) and in the left anterior descending artery distribution. When applied to a non-ACS cohort, the model had a specificity of 89% for ruling out the presence of CL precursors.

**TRANSLATIONAL OUTLOOK:** Future analysis is required in order to externally validate the ML model across various cohorts and to determine its generalizability. Such work has the potential to further enhance the ability for accurate phenotypic plaque characterization that precisely predicts at-risk individuals through the detection of CL precursors.

## REFERENCES

**1.** Virmani R, Kolodgie FD, Burke AP, et al. Atherosclerotic plaque progression and vulnerability to rupture: angiogenesis as a source of intraplaque hemorrhage. Arterioscler Thromb Vasc Biol 2005;25:2054–61.

**2.** Virmani R, Kolodgie FD, Burke AP, Farb A, Schwartz SM. Lessons from sudden coronary death: A comprehensive morphological classification scheme for atherosclerotic lesions. Arterioscler Thromb Vasc Biol 2000;20:1262–75.

**3.** Stone GW, Maehara A, Lansky AJ, et al. A prospective natural-history study of coronary atherosclerosis. N Engl J Med 2011;364:226–35.

**4.** Naghavi M, Libby P, Falk E, et al. From vulnerable plaque to vulnerable patient: a call for new definitions and risk assessment strategies: Part II. Circulation 2003;108:1772–8.

**5.** Virmani R, Burke AP, Farb A, Kolodgie FD. Pathology of the vulnerable plaque. J Am Coll Cardiol 2006;47 8 Suppl:C13–8.

**6.** Park S-J, Kang S-J, Ahn J-M, et al. Visual-functional mismatch between coronary angiography and fractional flow reserve. J Am Coll Cardiol Intv 2012;5:1029–36.

**7.** Nair A, Margolis P, Kuban B, Vince DG. Automated coronary plaque characterisation with intravascular ultrasound backscatter: ex vivo validation. EuroIntervention 2007;3:113–20.

**8.** Mintz GS. Intravascular imaging of coronary calcification and its clinical implications. J Am Coll Cardiol Img 2015;8:461–71.

**9.** Benjamin EJ, Virani SS, Callaway CW, et al. Heart disease and stroke statistics - 2018 update: a report from the American Heart Association. Circulation 2018;137:E67–492.

**10.** Goff DC, Lloyd-Jones DM, Bennett G, et al. 2013 ACC/AHA Guideline on the Assessment of Cardiovascular Risk: a report of the American College of Cardiology/American Heart Association Task Force on Practice Guidelines. J Am Coll Cardiol 2014;63:2935–59.

**11.** Al'Aref SJ, Min JK. Cardiac CT: current practice and emerging applications. Heart 2019;105:1597–605.

**12.** Papadopoulou S-L, Neefjes LA, Schaap M, et al. Detection and quantification of coronary atherosclerotic plaque by 64-slice multidetector CT: a systematic head-to-head comparison with intravascular ultrasound. Atherosclerosis 2011;219:163–70.

**13.** Chang H-J, Lin FY, Lee S-E, et al. Coronary atherosclerotic precursors of acute coronary syndromes. J Am Coll Cardiol 2018;71:2511–22.

**14.** Mendis S, Thygesen K, Kuulasmaa K, et al. World Health Organization definition of myocardial infarction: 2008-09 revision. Int J Epidemiol 2011;40:139–46.

**15.** Min JK, Dunning A, Lin FY, et al. Rationale and design of the CONFIRM (COronary CT Angiography EvaluatioN For Clinical Outcomes: An InteRnational Multicenter) registry. J Cardiovasc Comput Tomogr 2011;5:84–92.

**16.** Leipsic J, Abbara S, Achenbach S, et al. SCCT guidelines for the interpretation and reporting of coronary CT angiography: a report of the Society of Cardiovascular Computed Tomography Guidelines Committee. J Cardiovasc Comput Tomogr 2014;8:342–58.

**17.** Lundberg SM, Allen PG, Lee S-I. A unified approach to interpreting model predictions. Paper presented at: 31st Conference on Neural Information Processing Systems; December 4–9, 2017; Long Beach, CA.

**18.** Cury RC, Abbara S, Achenbach S, et al. CAD-RADSTM Coronary Artery Disease – Reporting and Data System. An expert consensus document of the Society of Cardiovascular Computed Tomography (SCCT), the American College of Radiology (ACR) and the North American Society for Cardiovascular Imaging (NASCI). J Cardiovasc Comput Tomogr 2016;10:269–81.

**19.** Motoyama S, Ito H, Sarai M, et al. Plaque characterization by coronary computed tomography angiography and the likelihood of acute coronary events in mid-term follow-up. J Am Coll Cardiol 2015 Jul 28;66:337–46.

**20.** Calvert PA, Obaid DR, O'Sullivan M, et al. Association between IVUS findings and adverse outcomes in patients with coronary artery disease: the VIVA (VH-IVUS in Vulnerable Atherosclerosis) Study. J Am Coll Cardiol Img 2011;4:894–901.

**21.** Tian J, Ren X, Vergallo R, et al. Distinct morphological features of ruptured culprit plaque for acute coronary events compared with those with silent rupture and thin-cap fibroatheroma: a combined optical coherence tomography and intravascular ultrasound study. J Am Coll Cardiol 2014;63:2209–16.

**22.** Ferencik M, Mayrhofer T, Bittner DO, et al. Use of high-risk coronary atherosclerotic plaque detection for risk stratification of patients with stable chest pain: a secondary analysis of the PROMISE randomized clinical trial. JAMA Cardiol 2018;3:144–52.

**23.** Mach F, Baigent C, Catapano AL, et al. 2019 ESC/EAS Guidelines for the management of dyslipidaemias: lipid modification to reduce cardiovascular risk. Eur Heart J 2020;41:111–88.

**24.** Kolossváry M, Karády J, Szilveszter B, et al. Radiomic features are superior to conventional quantitative computed tomographic metrics to identify coronary plaques with napkin-ring sign. Circ Cardiovasc Imaging 2017;10:e006843.

**25.** Al'Aref SJ, Anchouche K, Singh G, et al. Clinical applications of machine learning in cardiovascular disease and its relevance to cardiac imaging. Eur Heart J 2019;40:1975–86.

**KEY WORDS** acute coronary syndrome, coronary computed tomography angiography, diameter stenosis, machine learning

**APPENDIX** For supplemental tables, please see the online version of this paper.